

Chapter 2

Molecular Structure: A Primer

2.1 The Basics

Unlike an atom, whose fine structure is completely determined by the behavior of its electrons, a molecule's structure largely depends on the degrees of freedom of the nuclei. The ability of molecules to rotate and vibrate makes their spectra fundamentally different than that of atoms. Because of these extra degrees of freedom, the internal energy of a molecule, E_M , is the sum of three parts; rotation (E_R), vibration (E_V), and electronic (E_E):

$$E_M = E_R + E_V + E_E. \quad (2.1)$$

The relative scale of these energies is shown in Fig. 2.1. As seen in the figure, the three energy contributions represent three distinct energies scales - rotation, the smallest scale, adds energies on the order of 10 cm^{-1} , vibration contributes energies on the order of 1000 cm^{-1} , and the electronic energy is on the order of $10,000 \text{ cm}^{-1}$. For this reason, it is acceptable to treat vibration as a perturbation to the electronic energy and rotation as a perturbation to vibration.

The electronic contribution to the energy, E_E , is the same as for atoms. Namely, it is the energy of the molecule's electrons moving in the potential created by the nuclei and the other electrons. While this contribution is considerably more difficult to calculate for molecules than atoms, it is conceptually no different and all of one's intuition from atoms can be properly applied.

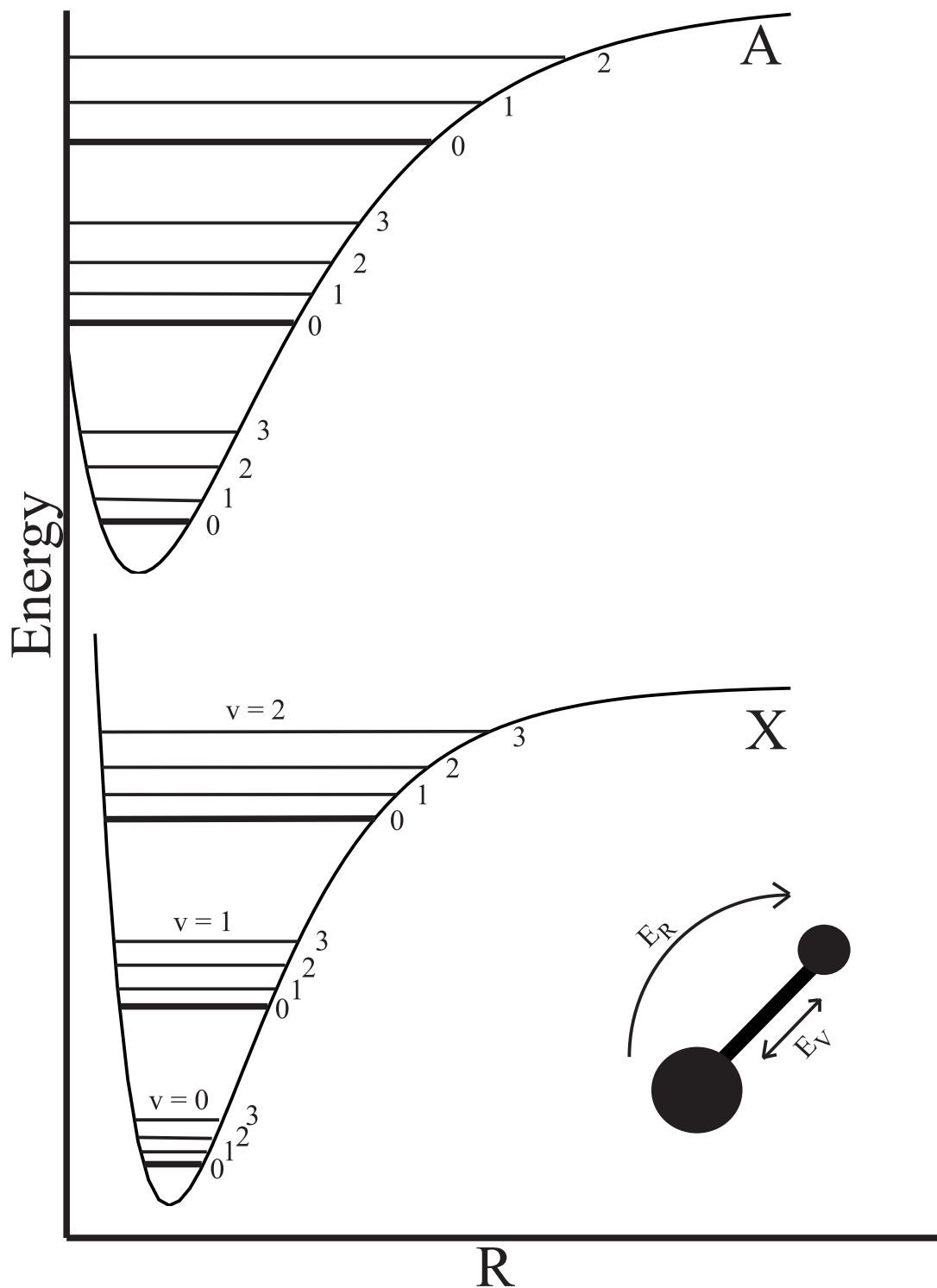


Figure 2.1: Schematic energy level structure of a molecule. The vibrational and rotational structure is drawn in the internuclear (Morse) potential for a ground (X) and excited (A) electronic state. Labels to the right of the potential curves are the rotational quantum number, R.

For low vibration and rotation, the intermolecular potential of Fig. 2.1 is sufficiently approximated as a harmonic oscillator [59]. Thus, the expected vibrational splittings are simply:

$$E_V = h\omega(v + 1/2), \quad (2.2)$$

where ω is the oscillator frequency and v is the vibrational quantum number. Clearly, as the molecule is excited in rotation and vibration this approximation breaks down, *i.e.* the vibrational potential becomes substantially anharmonic. To treat this, one typically expresses the vibrational energy of the molecule as a power series of harmonic oscillator energies with different oscillator frequencies,

$$E_V = \sum_n h\omega_n(v + 1/2)^n. \quad (2.3)$$

Retaining the first three terms of Eq. 2.3 is typically enough to be accurate within 1 cm^{-1} . Though the values of the ω_n 's can be calculated, they are usually derived from spectroscopic data.

The molecular rotation of a diatomic molecule can be approximated quite well by a rigid rotor model, which describes two masses m_1 and m_2 separated by a fixed distance, r . Solution of the rigid rotor Schrödinger equation yields the molecular rotation energies as:

$$E_R = \frac{h^2}{8\pi^2 I} R(R + 1), \quad (2.4)$$

where I is the molecule's moment of inertia and R is the rotational quantum number. The prefactor of Eq. 2.4 is called the rotational constant and is usually written as B for diatomic molecules. For a real vibrating molecule, the rigid rotor model breaks down since the average internuclear distance depends on v . However, by defining a value of B for each vibrational level, *i.e.* B_v , it is possible to use Eq. 2.4 to predict reasonably accurate values for the rotational energy spacing.

2.2 The Structure of OH

The neutral hydroxyl free radical (OH), though extremely chemically reactive, is a stable, diatomic molecule. For low rotational levels, the angular momentum coupling of the ${}^2\Pi$ electronic ground state of the OH molecule is sufficiently described by Hund's case (a) [59] as seen in Fig. 2.2. Under this interaction scheme, both the electron orbital angular momentum L and electron spin S are coupled to the intramolecular axis, leading to the definition of the total electron angular momentum as $\Omega = \Lambda + \Sigma$, where $|\Lambda| = 1$ ($|\Sigma| = 1/2$) represents the projection of L (S) onto this axis. This coupling results in two spin-orbit states, where the ${}^2\Pi_{3/2}$ state lies $\sim 126 \text{ cm}^{-1}$ below the ${}^2\Pi_{1/2}$ state as shown in Fig. 2.4(a). Strong spin-orbit coupling ($A_{SO} = -139 \text{ cm}^{-1}$) is responsible for the observed large splitting between the two Ω branches. The molecular angular momentum, J , in the laboratory frame is defined as $J = L + S + R$, where R represents the nuclear rotation angular momentum. The allowed values of J in the laboratory frame are given as $J = \Omega, \Omega + 1, \Omega + 2, \dots$

The fine structure energy in Hund's case (a) for a diatomic molecule is primarily given by the sum of the rotational energy described by the Hamiltonian H_{Rot} and the fine-structure energy described by the Hamiltonian H_{FS} . The rotational Hamiltonian is clearly given as

$$\begin{aligned}
 H_{Rot} &= B\vec{R}^2 \\
 &= B[(J^2 - J_z^2) + (L^2 - L_z^2) + (S^2 - S_z^2) + (L^+S^- + L^-S^+) \\
 &\quad - (J^+L^- + J^-L^+) - (J^+S^- + J^-S^+)], \tag{2.5}
 \end{aligned}$$

where subscript-z denotes the projection onto the space-fixed axis z (see Fig. 2.2). While the fine-structure Hamiltonian is the sum of two parts describing the spin-orbit and the spin-rotation coupling [144]

$$H_{FS} = A_{SO}\vec{L} \cdot \vec{S} + \gamma_{SR}\vec{R} \cdot \vec{S}$$

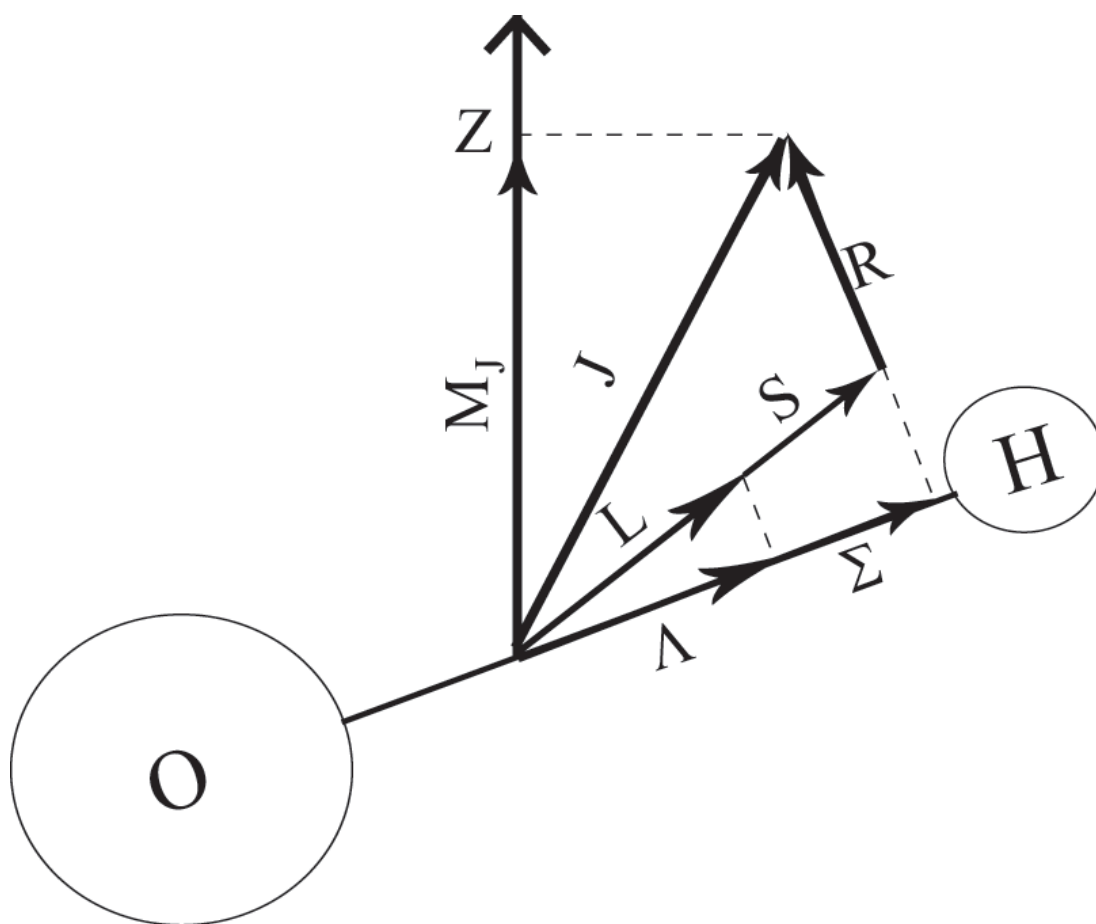


Figure 2.2: Hund's case (a) angular momentum coupling scheme for OH.

$$\begin{aligned}
&= A_{SO}L_zS_z + \frac{1}{2}A_{SO}(L^+S^- + L^-S^+) \\
&\quad + \gamma_{SR}(\vec{J} - \vec{L} - \vec{S}) \cdot \vec{S},
\end{aligned} \tag{2.6}$$

where γ_{SR} is the spin-rotation constant. The total Hamiltonian can efficiently be written in a Hund's case (a) basis that respects parity

$$|JM|\Omega|\epsilon\rangle = \frac{1}{\sqrt{2}}[|JM|\Omega\rangle|\Lambda\Sigma\rangle + \epsilon|JM - |\Omega\rangle| - \Lambda - \Sigma\rangle], \tag{2.7}$$

with the rotational part of the wavefunction given by the Wigner rotation matrix elements [31]

$$|JM\Omega\rangle = \left(\frac{2J+1}{8\pi^2}\right)^{\frac{1}{2}} D_{M\Omega}^{J*}(\theta, \phi, \chi). \tag{2.8}$$

In this basis, the matrix elements of the rotational Hamiltonian are given as

$$\begin{aligned}
E_{11}(J, \epsilon) &= \langle JM\frac{1}{2}\epsilon|H_{Rot}|JM\frac{1}{2}\epsilon\rangle = -\frac{1}{2}A_{SO} + B(J + \frac{1}{2})^2 \\
&\quad + \frac{1}{2}(1 - \epsilon(J + \frac{1}{2}))[p + q(1 - \epsilon(J + \frac{1}{2}))]
\end{aligned} \tag{2.9}$$

$$\begin{aligned}
E_{22}(J, \epsilon) &= \langle JM\frac{3}{2}\epsilon|H_{Rot}|JM\frac{3}{2}\epsilon\rangle = \frac{1}{2}A_{SO} + B((J + \frac{1}{2})^2 - 2) \\
&\quad + \frac{1}{2}q((J + \frac{1}{2})^2 - 1)
\end{aligned} \tag{2.10}$$

$$\begin{aligned}
E_{12}(J, \epsilon) &= \langle JM\frac{1}{2}\epsilon|H_{Rot}|JM\frac{3}{2}\epsilon\rangle = \\
&\quad -\frac{1}{4}[4B + p + 2q(1 - \epsilon(J + \frac{1}{2}))]\sqrt{(J + \frac{1}{2})^2 - 1},
\end{aligned} \tag{2.11}$$

where p and q are the Λ -doubling parameters. Diagonalizing this Hamiltonian leads to an intermediate Hund's case, *i.e.* mixture of Hund's case (a) states, with eigenstates

$$|\Psi^-\rangle = -b(J)|JM\frac{1}{2}\epsilon\rangle + a(J)|JM\frac{3}{2}\epsilon\rangle \tag{2.12}$$

$$|\Psi^+\rangle = a(J)|JM\frac{1}{2}\epsilon\rangle + b(J)|JM\frac{3}{2}\epsilon\rangle \tag{2.13}$$

$$a(J) = \left[\frac{\sqrt{4(J + \frac{1}{2})^2 + \frac{A_{SO}}{B}(\frac{A_{SO}}{B} - 4)} + (\frac{A_{SO}}{B} - 2)}{2\sqrt{4(J + \frac{1}{2})^2 + \frac{A_{SO}}{B}(\frac{A_{SO}}{B} - 4)}} \right]^{1/2} \tag{2.14}$$

$$b(J) = \left[\frac{\sqrt{4(J + \frac{1}{2})^2 + \frac{A_{SO}}{B}(\frac{A_{SO}}{B} - 4)} - (\frac{A_{SO}}{B} - 2)}{2\sqrt{4(J + \frac{1}{2})^2 + \frac{A_{SO}}{B}(\frac{A_{SO}}{B} - 4)}} \right]^{1/2}. \tag{2.15}$$

In Fig. 2.3, the values for the mixing coefficients, $a(J)$ and $b(J)$, are shown. At low J , $b(J)$ is nearly 1 and $a(J)$ is nearly 0, and thus $|\Psi^+\rangle \approx -|JM\frac{1}{2}\epsilon\rangle$ and $|\Psi^-\rangle \approx |JM\frac{3}{2}\epsilon\rangle$, which means that for low rotation OH is sufficiently described by a Hund's case (a) basis. For this reason, it is customary to label the OH states using a Hund's case (a) basis – though it is technically correct only for the lowest J levels where Ω is still a reasonable quantum number.

The energies of these eigenstates are given from the diagonalization of the 2×2 matrix of Eq. 2.11 as

$$E^\pm(J, \epsilon) = \frac{E_{11}(J, \epsilon) + E_{22}(J, \epsilon)}{2} \pm \frac{1}{2} \sqrt{(E_{11}(J, \epsilon) + E_{22}(J, \epsilon))^2 - 4(E_{11}(J, \epsilon)E_{22}(J, \epsilon) - E_{12}(J, \epsilon)^2)}, \quad (2.16)$$

where the \pm is the energy of the corresponding eigenstate in Eq. 2.15. From Eq. 2.16 the energies of the rotational states of OH can be calculated and are shown in Fig. 2.4. The relatively large energy splitting between J states is due to the small moment of inertia of the molecule and subsequent large rotational constant, B . The coupling between the nuclear rotation and the electron angular momentum (projection of L along the internuclear axis) results in Λ -type splitting (Ω -doubling) of each state, denoted as f and e states or in terms of the case a symmetry index as $\epsilon = +1$ and $\epsilon = -1$ (the parity of a state is given as $\epsilon(-1)^{J-1/2}$). In Fig. 2.4(b), these energy separations are exaggerated for clarity. For the most abundant isotopomer (^{16}OH) with an intrinsic nuclear spin, I of $1/2$, the free radical molecule is a boson. The total angular momentum is given by $F = I + J$. Each Λ -doublet component is split into hyperfine states that are characterized by a symmetry index p that defines the state's parity (\pm). The hyperfine energy separations have also been exaggerated for clarity of presentation in Fig. 2.4(b).

The vibrational structure of OH is the familiar spectrum of a diatomic molecule, which can be calculated from Eq. 2.3 using the values shown in Tab. 2.1.

The $^2\Sigma_{1/2}^+$ first electronic excited state of the OH molecule has an electron spin

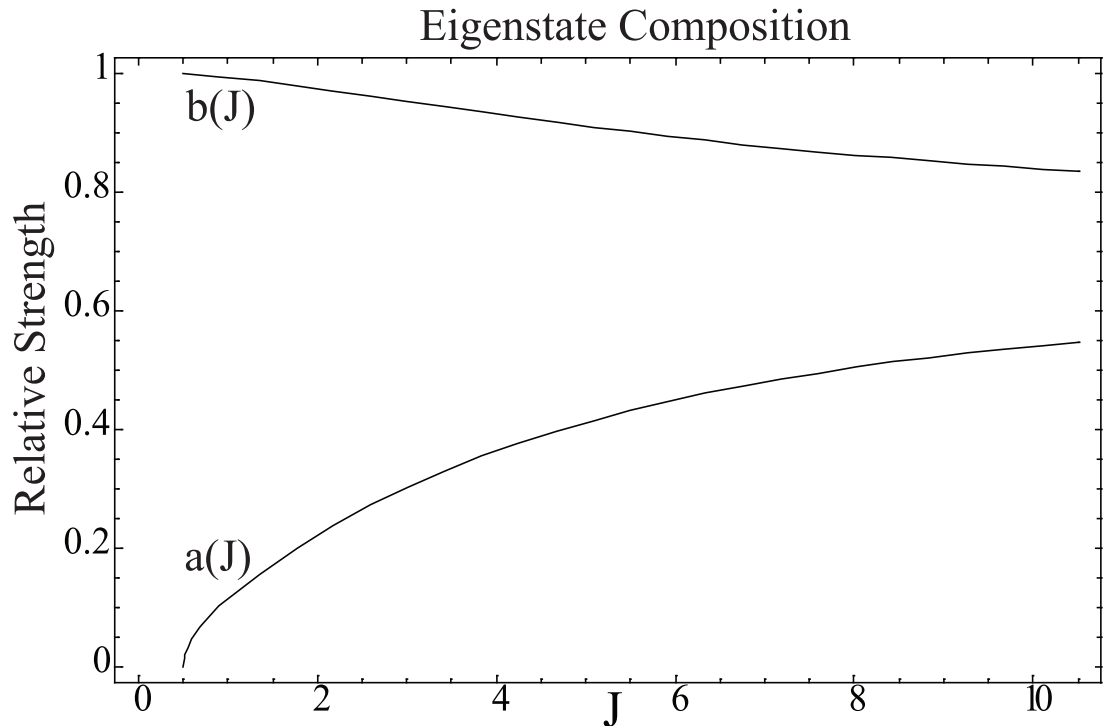


Figure 2.3: Mixing of the Hund's case (a) basis. At low J , $b(J)$ is nearly 1 and $a(J)$ is nearly 0 making it possible to label the states in the Hund's case (a) basis.

Table 2.1: Relevant molecular constants in units of cm^{-1} for calculating the ro-vibrational spectrum of OH. Taken from Refs. [36, 83].

	$v = 0$	$v = 1$	$v = 2$
B	18.531041	17.820121	17.118694
p	0.235214756	0.22462668	0.21387549
q	$3.86786223(10^{-2})$	$3.692540(10^{-2})$	$3.516101(10^{-2})$
ω_1	3737.7613		
ω_2	-84.881297		
ω_3	0.54090394		

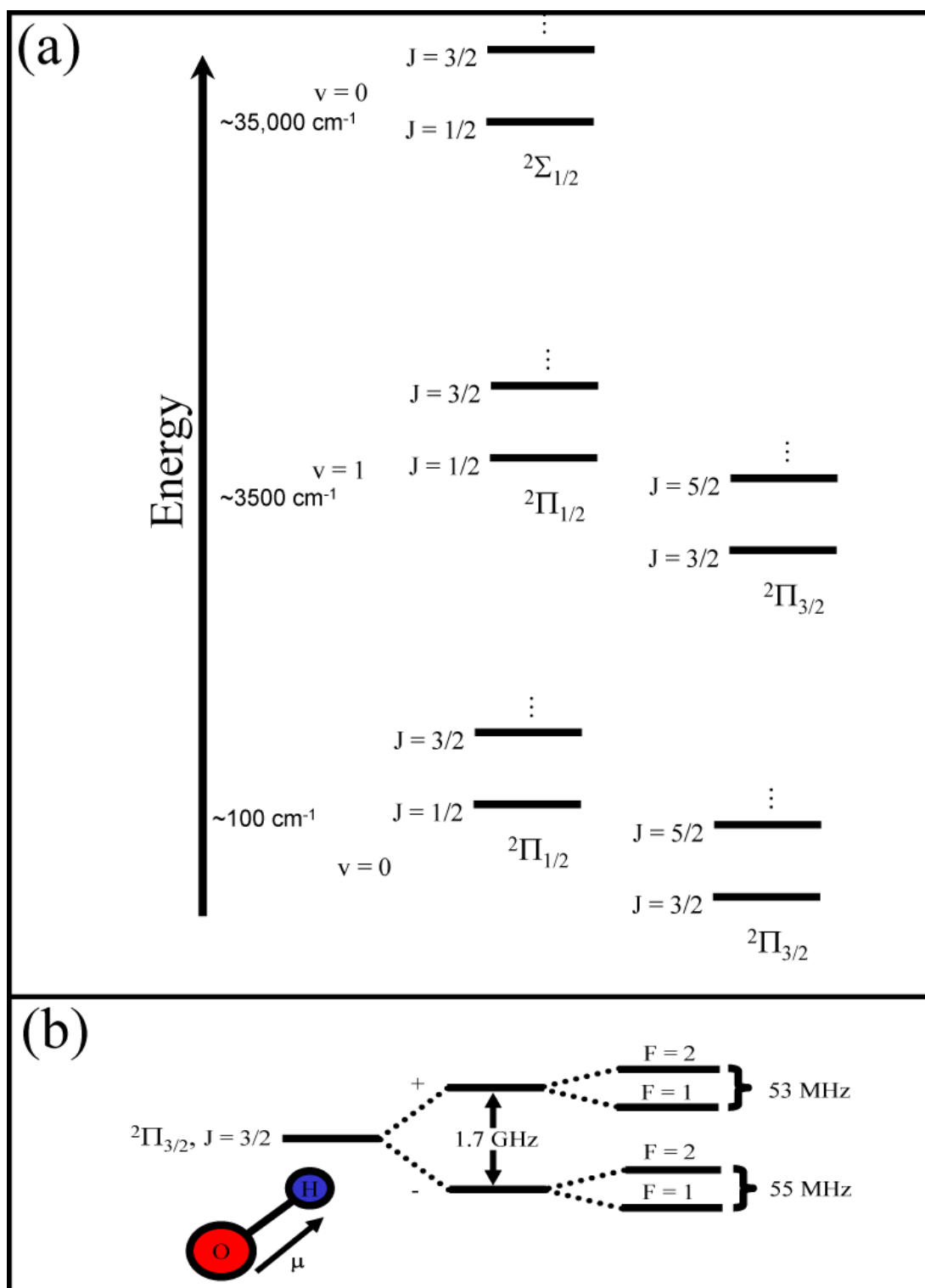


Figure 2.4: (a) Basic OH energy structure with both Λ - and ρ -doubling suppressed for clarity. The relative energy scale is given on the left. (b) Energy structure of $2\Pi_{3/2}$ ro-vibrational ground state of OH.

of 1/2 but no electron angular momentum; thus, the appropriate couplings are well-described by Hund's case (b) [59]. For this angular momentum configuration, the only important interaction is between the nuclear rotation of the molecule R and the electron spin S – so-called ρ -doubling. This coupling separates every J state that has non-zero R into two states of the same parity and like the Λ -doubling of the Π state has been suppressed in Fig. 2.4(a) for clarity.

Because the Λ -doublet states possess opposite parity and small energy separations, adjacent levels of the ground state OH readily mix under the interaction of the molecule's permanent electric dipole ($\mu = 1.67$ D) with an external electric field. Since the electric dipole moment, μ , must lie along the intermolecular axis, its projection on the space fixed axis z , *i.e.* the electric field, is given as

$$\mu_{eff} = \mu \cos(\Omega, J) \cos(J, z) = \mu \frac{\Omega}{\sqrt{J(J+1)}} \frac{M_J}{\sqrt{J(J+1)}} = \frac{\mu \Omega M_J}{J(J+1)}, \quad (2.17)$$

where $\cos(a, b)$ is the interior angle between vectors \vec{a} and \vec{b} . The matrix elements of this dipolar coupling for a linear electric field, transformed into a hyperfine basis, are given by [87]

$$\begin{aligned} \langle JI|\Omega|FM_F\epsilon|\vec{\mu} \cdot \vec{\mathbf{E}}|J'I'|\Omega'|F'M'_F\epsilon'\rangle &= -\frac{\mu E}{2} [1 + (-1)^{J+J'} \epsilon\epsilon'] (-1)^{F+F'+M'_F+I-|\Omega|+1} \\ &\times \sqrt{[J][J'][F][F']} \begin{pmatrix} J & 1 & J' \\ -|\Omega| & 0 & |\Omega| \end{pmatrix} \begin{pmatrix} F' & 1 & F \\ -M'_F & 0 & M_F \end{pmatrix} \begin{Bmatrix} J & 1 & J' \\ -|\Omega| & 0 & |\Omega| \end{Bmatrix}. \end{aligned}$$

Inspection of the above equation reveals the convenient fact that only states of the same Ω and M_F are coupled. With the large spin-orbit and rotational splittings present in OH, this means that the Stark shifts of the relevant states are accurately calculated with a basis containing only the lowest Λ -doublet. For example, the Stark shift of four of the main states of interest, $|2 \pm 2 \pm\rangle$ ($|FM_Fp\rangle$) (the stretched states), is given from the Hamiltonian:

$$H^{Stark} = \begin{pmatrix} 0 & -\frac{3}{5}\mu E \\ -\frac{3}{5}\mu E & \Delta_\Lambda \end{pmatrix}, \quad (2.18)$$

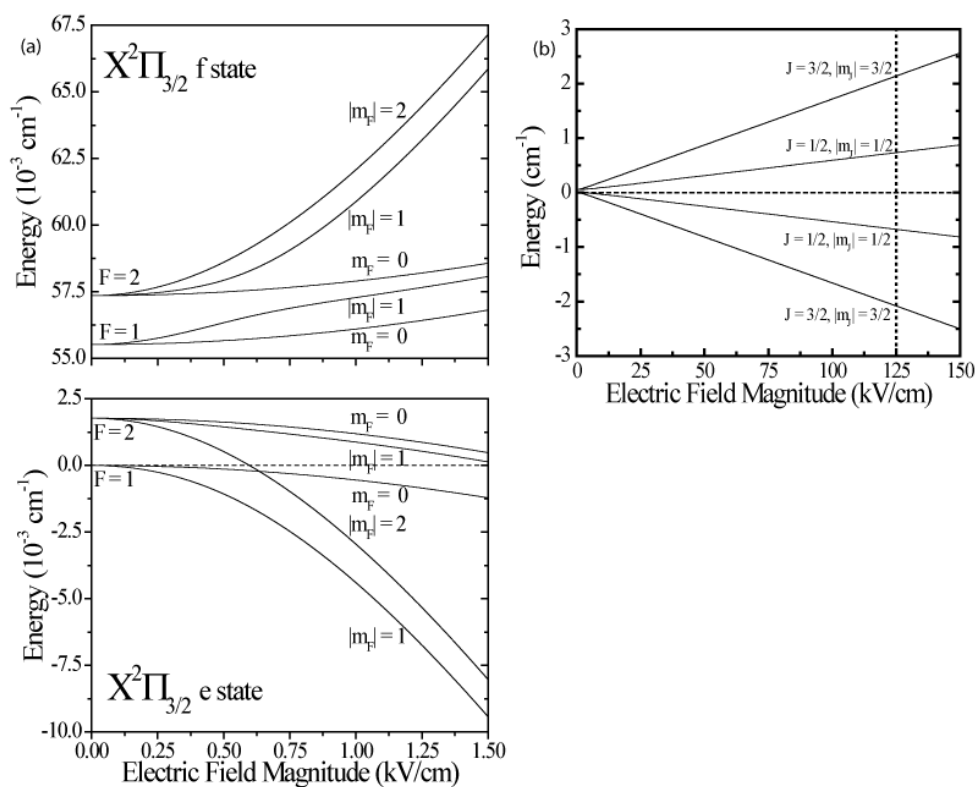


Figure 2.5: (a) The Stark energy shift for ground state OH molecules in low electric fields. The initial e (f) state is shown in the lower (upper) panel, where the hyperfine levels are indicated next to the traces. (b) The Stark shift for ground state OH molecules in high electric fields. The vertical dotted line indicates the regime where the Stark decelerator operates; the dashed horizontal line denotes zero energy.

written in the basis

$$\Psi = \begin{pmatrix} |2 \pm 2-\rangle \\ |2 \pm 2+\rangle \end{pmatrix}. \quad (2.19)$$

And thus, the Stark shift of these state is $E_{Stark}^{\pm} = \frac{\Delta\Lambda}{2} \pm \sqrt{(\frac{\Delta\Lambda}{2})^2 + (\frac{3}{5}\mu E)^2}$ and the eigenvectors are given as

$$|\chi^{\pm}\rangle = \frac{1}{\sqrt{(\frac{3}{5}\mu E)^2 + (E_{Stark}^{\pm})^2}} \left(\left(\frac{-3}{5}\mu E \right) |2 \pm 2-\rangle + E_{Stark}^{\pm} |2 \pm 2+\rangle \right). \quad (2.20)$$

The energy of these mixed states increases (weak-field seeking states) or decreases (strong-field seeking states) as a function of the electric field strength, as shown for the ro-vibrational ground state of OH in Fig. 2.5. The Stark energy shift evolves from quadratic to linear when the energy change due to the applied field exceeds the Λ -doublet splitting value of 0.055 cm^{-1} . The ground state shift is unaffected by the next higher rotational state due to the large energy separation of $\sim 84 \text{ cm}^{-1}$.

In the high electric field regime, the complex energy levels depicted in Fig. 2.5(a) emerge as four distinct fine-structure families. As shown in Fig. 2.5(b), for the Stark slowing experiment discussed here, the weak-field seeking states are most relevant, with the ${}^2\Pi_{3/2} F = 2, -m_F = 2, 1$ states experiencing approximately three times the Stark energy shift of the ${}^2\Pi_{3/2} F = 2, m_F = 0$ and ${}^2\Pi_{3/2} F = 1, m_F = 0, 1$ states. The horizontal dashed line corresponds to the zero energy level while the vertical dotted line represents the peak electric field magnitude under the normal operating voltages of the Stark decelerator. We note molecules in strong-field seeking states do not survive the first state-selection device, namely the hexapole acting as a molecular focusing lens, and therefore do not contribute to any observed signals thereafter.

From the eigenstates of Eq. 2.20 we calculate the expectation value for the electric dipole moment as a function of an electric field as

$$\langle \chi^{\pm} | \mu | \chi^{\pm} \rangle = \frac{-1}{(\frac{3}{5}\mu E)^2 + (E_{Stark}^{\pm})^2} \left(\left(\frac{3}{5}\mu E \right) E_{Stark}^{\pm} \langle 2 \pm 2 + | \mu | 2 \pm 2 - \rangle \right)$$

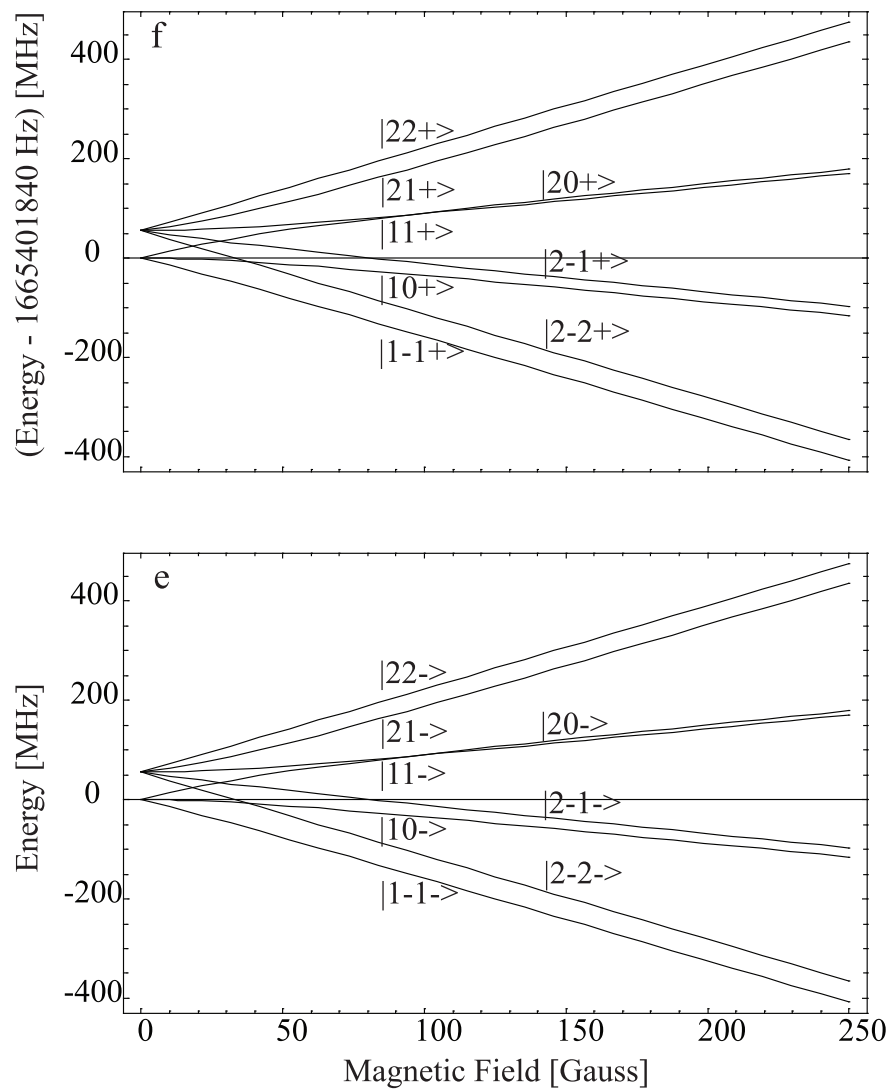


Figure 2.6: (a) The Zeeman energy shift for ground state OH molecules in low magnetic fields. The initial e (f) state is shown in the lower (upper) panel, where the hyperfine levels are indicated next to the traces.

$$\begin{aligned}
& + \left(\frac{3}{5} \mu E \right) E_{Stark}^{\pm} \langle 2 \pm 2 - |\mu| 2 \pm 2 + \rangle \\
& = -\frac{18}{25} \left(\frac{(\mu E) E_{Stark}^{\pm}}{(\mu E)^2 + (E_{Stark}^{\pm})^2} \right) \mu.
\end{aligned} \tag{2.21}$$

A graph of the OH dipole moment according to this equation is shown in Fig. 2.7. The signature of a ‘permanent-electric dipole moment’ is evident; as the field is increased from zero the dipole moment increases from zero until it reaches its asymptotic value. At this point the dipole moment is said to be saturated, and the Stark shift becomes linear. Since the dipole-dipole potential, which depends on μ , is the dominant interaction between colliding polar molecules this leads to electric field dependent collision properties as detailed in Chap. 10.

Similarly, the Zeeman shift of the lower Λ -doublet in OH can be calculated by considering a basis that contains only the lowest Λ -doublet states. Since a Hund’s case (a) molecule’s electronic spin and orbital angular momentum are strongly coupled to the intermolecular axis, OH possesses a magnetic dipole moment along its intermolecular axis of $\mu_{Bo} = \mu_b(\Lambda + g_e \Sigma)$ (μ_b is the Bohr magneton and $g_e = 2.002$). Like the case of an electric dipole moment this leads to a projection on the space-fixed axis, *i.e.* magnetic field, of

$$\mu_{Bo,eff} = \frac{\mu_b(\Lambda + g_e \Sigma) \Omega M_J}{J(J+1)}. \tag{2.22}$$

The matrix elements of this dipolar coupling for a linear magnetic field, transformed into a hyperfine basis, are given by [122]

$$\begin{aligned}
\langle JI|\Omega|FM_F\epsilon|\vec{\mu} \cdot \vec{\mathbf{B}}|J'I'|\Omega'|F'M'_F\epsilon'\rangle & = -\frac{(\Lambda+g_e\Sigma)B}{2}[1+(-1)^{J+J'+2|\Omega|}\epsilon\epsilon'](-1)^{J+J'+F+F'-M_F+I-|\Omega|} \\
& \times \sqrt{[J][J'][F][F']} \begin{pmatrix} J & 1 & J' \\ -|\Omega| & 0 & |\Omega| \end{pmatrix} \begin{pmatrix} F' & 1 & F \\ M'_F & 0 & -M_F \end{pmatrix} \begin{Bmatrix} F & F' & 1 \\ J' & J & I \end{Bmatrix}.
\end{aligned}$$

Conveniently, the magnetic dipole operator does not couple states of the opposite parity and the upper and lower Λ -doublet have essentially the same Zeeman shift as shown in Fig. 2.6.

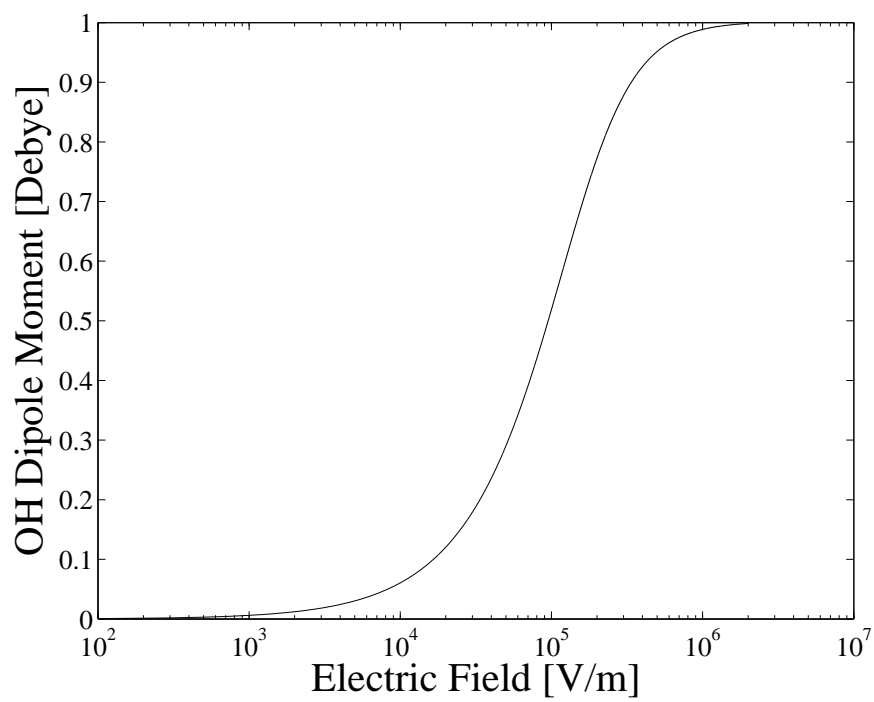


Figure 2.7: The absolute value of the of the OH dipole moment for the $|2 \pm 2\pm\rangle$ state.

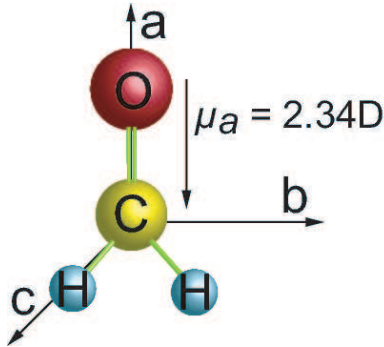


Figure 2.8: Structure of formaldehyde (H_2CO).

2.3 The Structure of H_2CO

As shown in Fig. 2.8, H_2CO is a near-symmetric prolate top molecule, with nearly degenerate rotations about the b- and c- axes. The dipole moment, μ_a , along the a-axis causes these nearly degenerate, opposite parity states to experience a large Stark shift with an applied electric field. Calculations of the Stark shift are quite intense since there is no analytical expression for the zero-field energies of asymmetric top molecules. The rotational Hamiltonian for the asymmetric rotor can be written as [56]:

$$H = A\mathbf{J}_a^2 + B\mathbf{J}_b^2 + C\mathbf{J}_c^2, \quad (2.23)$$

where A, B, and C are the rotational constants for rotation about the respective axes and \mathbf{J}_i^2 is the angular momentum operator for the i th axis. Since the rotational energy of a symmetric top molecule is well known [123], it is convenient to recast Eq. 2.23 into two terms – one of which is diagonal in the symmetric top basis and one that couples different symmetric top states:

$$H = 1/2(A + C)\mathbf{J}^2 + 1/2(A - C)(\mathbf{J}_a^2 + \frac{2B - A - C}{A - C}\mathbf{J}_b^2 - \mathbf{J}_c^2). \quad (2.24)$$

Thus, the problem of calculating the rotational energies of an asymmetric top molecule has been reduced to diagonalizing Eq. 2.24 in the symmetric top molecule basis of

Table 2.2: Parameters for calculating the off-diagonal rotational contribution for an asymmetric top molecule.

Principal axis	a	b	c
F	$\frac{1}{2}\left(\frac{2B-A-C}{A-C} - 1\right)$	0	$\frac{1}{2}\left(\frac{2B-A-C}{A-C} + 1\right)$
G	1	$\frac{2B-A-C}{A-C}$	-1
H	$-\frac{1}{2}\left(\frac{2B-A-C}{A-C} + 1\right)$	1	$\frac{1}{2}\left(\frac{2B-A-C}{A-C} - 1\right)$

$|JKM\rangle$, where K is the projection of J onto the symmetric top molecule's symmetry axis. Schematically, the rotational energy and eigenstates of the asymmetric top molecule in the $|J_\tau M\rangle$ ($\tau = K_a - K_c$) basis may now be written as:

$$E_{J_\tau M} = \frac{1}{2}(A + C)J(J + 1) + \frac{1}{2}(A - C)\tilde{E}_{J_\tau M} \quad (2.25)$$

$$|J_\tau M\rangle = \sum_K a_K^{J_\tau M} |JKM\rangle, \quad (2.26)$$

where both the values $a_K^{J_\tau M}$ and $\tilde{E}_{J_\tau M}$ are found from the eigenvalues and eigenvectors of the non-diagonal part of Eq. 2.24. The matrix elements of this part of the Hamiltonian can be found in several reviews [56, 123], and are given as:

$$\begin{aligned} \langle JKM | \mathbf{J}_a^2 + \frac{2B-A-C}{A-C} \mathbf{J}_b^2 - \mathbf{J}_c^2 | JKM \rangle &= F[J(J + 1) - K^2] + GK^2 \\ \langle J(K \pm 2)M | \mathbf{J}_a^2 + \frac{2B-A-C}{A-C} \mathbf{J}_b^2 - \mathbf{J}_c^2 | JKM \rangle &= \\ H \sqrt{\frac{1}{4}[J(J + 1) - K(K \pm 1)][J(J + 1) - K(K \pm 1)(K \pm 2)]}, \end{aligned}$$

where the values of F, G, and H depend on the molecule's principal axis, *i.e.* the molecule's axis of symmetry in the symmetric top limit, and are given in Tab. 2.2. As seen in Fig. 2.8, H₂CO is a type-a molecule and the appropriate values for F, G, and H are taken from the first column of Tab. 2.2.

Once the zero-field energies and eigenstates of the asymmetric top rotor are found, *i.e.* once eqns. 2.25 and 2.26 are solved, the Stark effect of an electric field, E , may be calculated from the Hamiltonian:

$$H_{Stark} = E \sum_i \mu_i \Phi_i, \quad (2.27)$$

Table 2.3: Direction cosine reduced matrix elements

Matrix Element	$J' = J + 1$	J	$J' = J - 1$
$\langle J \Phi_i J'\rangle$	$\frac{1}{4(J+1)\sqrt{(2J+1)(2J+3)}}$	$\frac{1}{4J(4J+1)}$	$\frac{1}{4J\sqrt{4J^2-1}}$
$\langle JM \Phi_i J'M\rangle$	$2\sqrt{(J+1)^2 - M^2}$	$2M$	$-2\sqrt{J^2 - M^2}$
$\langle JK \Phi_i J'K\rangle$	$2\sqrt{(J+1)^2 - K^2}$	$2K$	$-2\sqrt{J^2 - K^2}$

where μ_i is the dipole moment along the i th axis and Φ_i is the direction cosine between the electric field direction and the i th axis. The direction cosine matrix elements are given in the $|J_\tau M\rangle$ basis as:

$$\langle J_\tau M|\Phi_i|J'_\tau M\rangle = \langle J|\Phi_i|J'\rangle \langle JM|\Phi_i|J'M\rangle \sum_K a_K^{J_\tau M} a_K^{J'_\tau M} \langle JK|\Phi_i|J'K\rangle, \quad (2.28)$$

with the values of the reduced matrix elements given in Tab. 2.3.

For H₂CO only the a-axis supports a dipole moment, and thus the Stark effect is conceptually similar to a diatomic molecule like OH. However, unlike the OH case, where different Λ -doublet states are coupled by the electric field, different J states are coupled in H₂CO and thus a large basis of states is required to accurately approximate the Stark shift. The results of a calculation that included up to $J = 3$ (16 basis states) are shown in Fig. 2.9. Here, the states are labeled by their zero-field identity in the $|J_\tau m_J\rangle$ basis. Of particular interest to this work is the $|1_1 1\rangle$ state, which is the upper component of the lowest J level of ortho-formaldehyde and is hence well populated in our supersonic expansion. This state experiences a large Stark shift (1.32 cm^{-1} at 125 kV/cm), making it excellent for Stark deceleration. There are other states accessible via, for example, stimulated Raman adiabatic passage that offer an improved Stark deceleration efficiency ($|2_2 2\rangle$) or a good candidate for implementing an AC Stark trap ($|0_0 0\rangle$) [129].

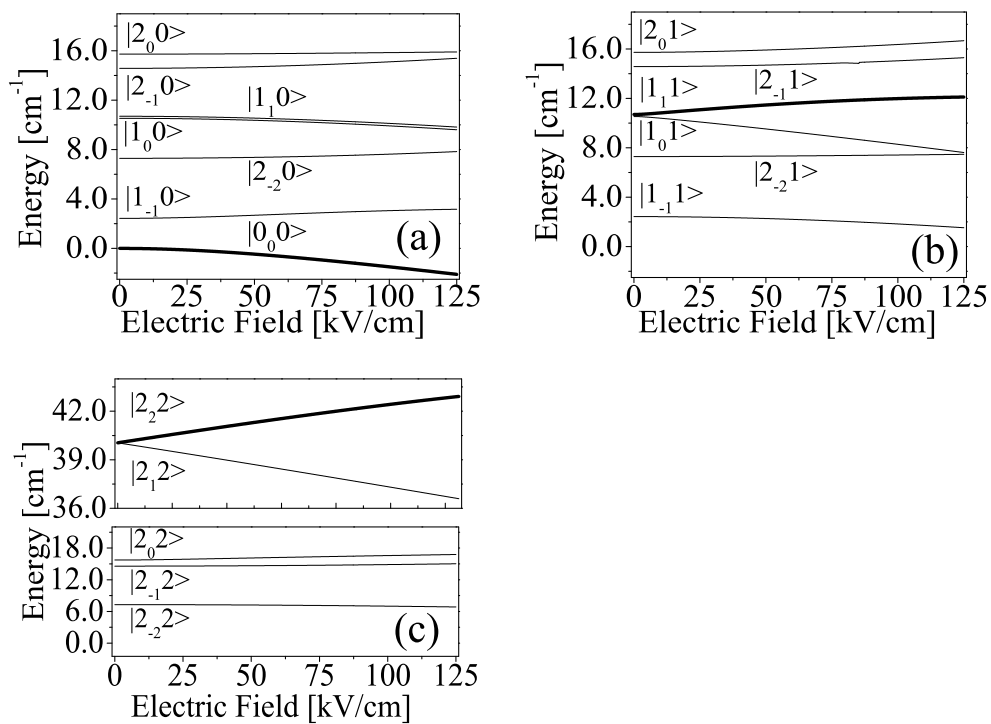


Figure 2.9: Stark shifts of the low-lying rotational states of H₂CO. States of interest for Stark deceleration and trapping are shown in bold.